Performance of Multipurpose Detectors in Super B Factories

G. Eigen*
University of Bergen

Based on background measurements at PEP II the impact of machine-related backgrounds on individual components of multipurpose detectors is examined, that operate in an asymmetric B factory at luminosities up to 10^{36} cm^{-2}s^{-1}. Extrapolations of the BABAR experience suggests two feasible detector designs.

1. Introduction

CP violation in the B system has been observed recently by BABAR [1] and BELLE [2]. In a 30.5 fb^{-1} sample BABAR measured $\sin 2\beta = 0.59 \pm 0.14 \pm 0.05$. In order to achieve high-precision measurements of all angles in the Unitarity Triangle [3], and to precisely measure branching fractions, *CP* asymmetries and forward-backward asymmetries in rare B decays [3], [4] very high luminosities (10 ab^{-1}/y) are a prerequisite. Recently, an e^+e^- asymmetric super B factory has been proposed that operates at peak luminosities of $\mathcal{L}_{peak} = 10^{36}$ cm^{-2}s^{-1} [5]. This is a factor of ~ 250 higher than presently achieved in PEP II and KEKB. To maintain 10^{36} cm^{-2}s^{-1} continuous injection becomes necessary since beam life times are rather short. This imposes new running conditions on the detector because of enhanced machine-related backgrounds. In the following we examine the performance of individual subsystems of present multipurpose detectors in a high-radiation environment. Using parameterizations that were established in a PEP II luminosity-upgrade study and are based on measurements at 3×10^{33} cm^{-2}s^{-1} [6] we extrapolate quantities affected by machine-related backgrounds to high luminosities. In addition to results presented in [6] we perform extrapolations to three high luminosity points: 5×10^{34} cm^{-2}s^{-1}, 1×10^{35} cm^{-2}s^{-1} and 1×10^{36} cm^{-2}s^{-1}. Our results have to be taken with a grain of salt, since extrapolations are carried out over 1-2 orders of magnitude and are very specific to the present layout of the PEP II interaction region (IR). Nevertheless, they are rather instructive and serve as a crude guideline.

2. Background Issues

Acceptable levels of radiation-induced backgrounds are determined by radiation hardness of the detector, occupancy and trigger rate. Radiation damage causes inefficiencies and eventually leads to the destruction of detectors. The total integrated dose, that determines the detector life time, is accumulated under normal running conditions, during injection, during machine studies and from beam-loss events. Injection losses in PEP II contribute only $25 - 30\%$ of the integrated dose in the SVT horizontal plane. Because of the continuous injection in the super B factory, it is important to ascertain that the detector is well-protected from injection losses. High levels of detector occupancies cause inefficiencies leading to lower resolutions and reduced signal/background ratios, whereas high trigger rates cause increased dead times and in turn a loss of signal events. Thus, acceptable detector occupancies and trigger rates determine dynamic running conditions of the experiment.

In PEP II machine-related backgrounds result from (i) electrons that produce lost particles via beam-gas bremsstrahlung and Coulomb scattering in addition to synchrotron radiation, (ii) positrons that produce lost-particles via beam-gas bremsstrahlung, Coulomb scattering and "tune-tails" and (iii) from beam-beam interactions, where the latter yields contributions from luminosity and beam-beam tails in the colliding mode. In the super B factory beam loss rates are

*eigen@asfys2.fi.uib.no

enhanced by a factor of $> 10^3$ as shown in Table I [7]. Here, the main sources are the Touschek effect and beam-beam tune shifts. We expect, however, that only a small fraction of the beam losses will contribute to backgrounds at the IR. For example, in PEP II the LER (HER) beam life time is determined by vacuum or the Touschek effect (beam-beam tune shift and second vacuum). The main background source in the silicon vertex tracker (SVT), the drift chamber (DCH) and the electromagnetic calorimeter (EMC), however, comes from beam-gas interactions in the PEP II incoming straight sections, which have a negligible effect on beam life times. Beam losses due to beam-beam tune shifts, dynamic aperture and vacuum probably will contribute to vacuum-like backgrounds, since they are transverse, similarly to distant Coulomb scattering of the LER beam in PEP II. Since there should be no aperture limitations very close to the IR (in particular not from the low-β quadrupoles), transverse losses are produced at betatron collimators far from the IR. Longitudinal losses such as the Touschek effect, whose background impact has not yet been studied at PEP II, probably behave like distant bremsstrahlung and may be collimated. Thus, according to Table I the combined transverse losses are the main issue of which $15-20\%$ result from the ring-averaged vacuum in the LER. As in PEP II, the vacuum pressure should be kept at $< 10^{-9}$ Torr within a few 10 m of the IR. Since the sum of longitudinal losses, all transverse losses and injection losses is so large, the background issue from vacuum at the IR is likely to be minor by comparison.

In order to estimate the background contributions due to different beam-loss effects and determine parameterizations in terms of beam currents and luminosity in a super B factory several studies are needed. Note that our extrapolations are at best order-of-magnitude estimates, especially at 10^{36} cm^{-2}s^{-1}, since we presently have no reliable procedure to include the effects of high beam losses in a super B factory.

Table I Background composition in PEP II and a super B factory [7]

	HER	LER	super HER	super LER
Beam current I_b [A]	0.7	1.4	5.5	20.5
Beam life time τ_b [min]	550	150	4.2	3.2
Luminosity [A/min]			0.37	0.35
Vacuum [A/min]			0.06	0.68
Touschek [A/min]			0.06	2.28
beam-beam tune shift [A/min]			0.55	2.55
Dynamic aperture [A/min]			0.28	1.03
Total beam loss rate I_b/τ_b [A/min]	1.3×10^{-3}	9.3×10^{-3}	1.3	6.4

3. Silicon Vertex Trackers (SVT)

Silicon vertex detectors, located closest to the beam, are exposed to the highest levels of radiation. The specific radiation dose depends both on beam currents and on the IR layout. In BABAR the horizontal plane is most affected due to the PEP II beam optics at the IR. Here the dose rate is a factor of ~ 5 larger than in other SVT regions. Figure 1 shows the presently accumulated dose rate in the BABAR SVT. The Si detectors are expected to survive at least a 2 Mrad radiation dose. Thus, with replacements of detectors in the horizontal plane the BABAR SVT should survive luminosities of $\mathcal{L} = 1.5 - 3.0\times10^{34}$ cm^{-2}s^{-1}. Dose rates in the horizontal plane (forward-east and backward-west) scale with LER and HER beam currents (in [A]) as [6]:

$$\begin{aligned} D_{SVT}\ [\mathrm{kRad/y}] &= 128\cdot I_{LER} + 16\cdot I_{LER}^2 \quad \text{(for FE MID plane)},\\ D_{SVT}\ [\mathrm{kRad/y}] &= 246\cdot I_{HER} + 9.1\cdot I_{HER}^2 \quad \text{(for BW MID plane)}. \end{aligned} \tag{1}$$

The dose rates in the horizontal plane projected for different luminosities are plotted in Figure 1 and are summarized in Table II. *R&D* studies in ATLAS [8] have demonstrated that silicon-strip detectors can survive very high radiation levels in hadronic environments. However, this requires cooling and the use of p^+nn^+ detectors, which are read out on the p^+ side. The radiation eventually changes n-type Si into p-type Si moving the depletion layer away from the readout plane

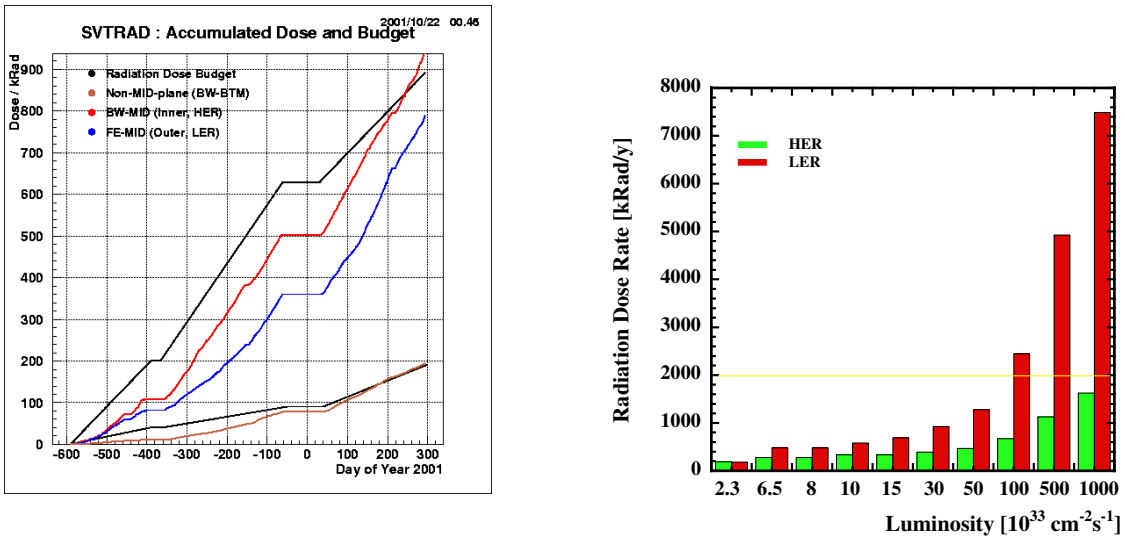

Figure 1: Dose accumulated in BABAR in the horizontal plane and other regions (left); projected dose rates in the horizontal plane for different $\mathcal{L}$ (right). The solid horizontal line shows the 2 Mrad dose limit for the BABAR SVT.

which costs a factor of ~ 2 in signal/noise [9]. This effect also occurs at a reduced rate in an electromagnetic radiation environment. At $\mathcal{L} = 10^{36}$ cm^{-2}s^{-1} occupancy is an issue for Si strip detectors. Thus, the first two layers need to be made of pixels. H. Yamamoto succeeded to bond 150 μm thick pixels (55 μm $\times$ 55 μm) using CMOS technology [10]. For the three outer layers Si strip detectors are fine. To determine the specific layout of the Si pixel and Si strip detectors, *R&D* studies are necessary. With the appropriate design Si detectors are expected to work in high-radiation environments.

4. Drift Chambers (DCH)

Machine backgrounds affect the operation of a drift chamber in three ways. First, the total current I_{DCH} drawn by the wires in the drift chamber is dominated by the charge released by beam-related showers and is limited by the high-voltage system. Above this limit the chamber becomes non-operational. Though this limit can be increased by adding power supplies, high currents also contribute to drift chamber aging. Permanent damage is expected to occur at charge-densities of $Q_{max} > 0.1$ C/cm of wire. Second, the occupancy in the drift chamber due to backgrounds can hamper the reconstruction of physics events. Third, ionization radiation can permanently damage read-out electronics and digitizing electronics.

Figure 2 shows the DCH currents measured in BABAR as a function of LER and HER beam currents for an operating high voltage of $U = 1900$ V. The best description of the high-current region is achieved with a linear plus quadratic fit for $I_{LER} > 700$ mA and $I_{HER} > 150$ mA. To extrapolate to high luminosities we use the following BABAR parameterizations of drift chamber currents and occupancies in terms of beam currents (in units of [A]) and luminosity (in units of [10^{33} cm^{-2}s^{-1}]) [6],

$$\begin{aligned} I_{DCH}[\mu A] &= 35.3 \cdot I_{LER} + 23.5 \cdot I_{LER}^2 + 77.2 \cdot I_{HER} + 46.3 \cdot I_{HER}^2 + 41.9 \cdot \mathcal{L} - 14, \\ N_{DCH}[\%] &= 0.044 + 0.191 \cdot I_{LER} + 0.0402 \cdot I_{LER}^2 + 1.03 \cdot I_{HER} + 0.113 \cdot I_{HER}^2 + 0.147 \cdot \mathcal{L}. \end{aligned} \quad (2)$$

The drift chamber currents, occupancies and charge densities accumulated on the wires extrapolated to high $\mathcal{L}$ for $U = 1900$ V are summarized in Table II. Figure 3 shows the individual contributions of drift chamber currents and occupancies due to beam currents and luminosity extrapolated for different luminosities. For $\mathcal{L} > 5 \times 10^{34}$ cm^{-2}s^{-1}, it is rather unlikely that a drift chamber will function. Thus, at $\mathcal{L} > 1 \times 10^{36}$ cm^{-2}s^{-1} other tracking devices have to be used. Candidates are Si-strip detectors, straw chambers and GEM detectors. Specific *R&D* is needed to

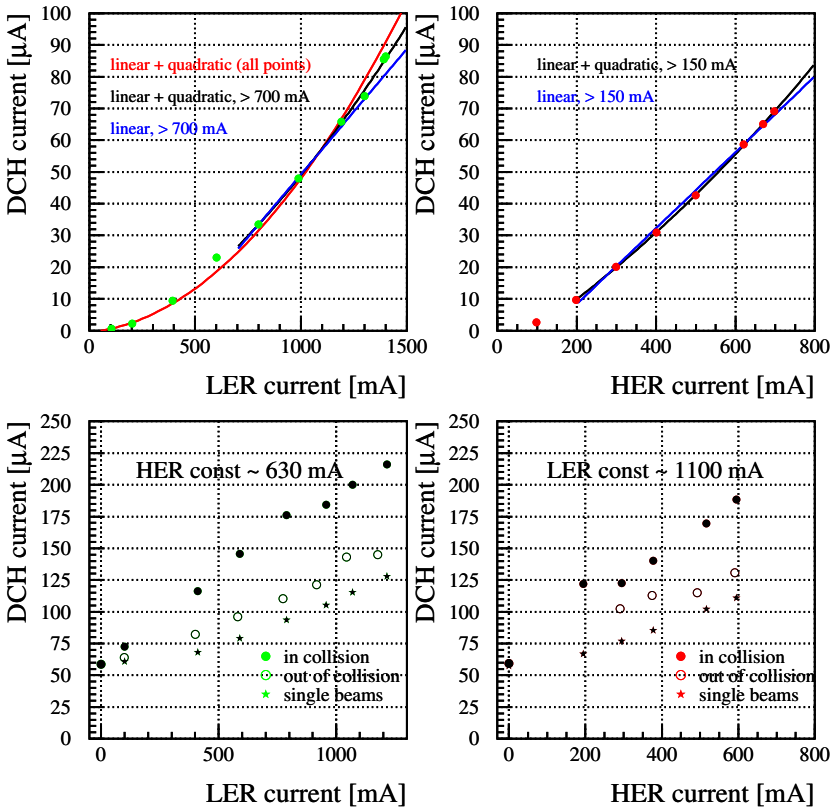

Figure 2: Drift chamber currents as a function of beam currents measured in BABAR. The solid lines show different fits.

find the optimal tracker in terms of layouts balancing multiple scattering versus position resolution and magnetic field strength versus track length. For example, a Si strip tracker would be integrated with the SVT. Here, multiple scattering is of concern. For a combined tracking system with two layers of Si pixel detectors and seven layers of Si strip detectors, which are each 200 μm thick, have a position resolution of 20 μm each and are positioned within a 50 cm radius, the momentum resolution in a 3 T magnetic field is $\sigma_{p_t}/p_t = 0.47\% \oplus 0.072 p_t\%$ (including a beam pipe). The multiple-scattering term is slightly worse than that in BABAR [11], where a momentum resolution of $\sigma_{p_t}/p_t = 0.45\% \oplus 0.13 p_t\%$ is measured. Including a mechanical support structure for the Si detectors the multiple-scattering term may increase by 20 – 30%.

5. DIRC Particle Identification

The main issue for the DIRC is occupancy. In BABAR the occupancy scales linearly with beam currents ([A]) and luminosity ([10^{33} cm$^{-2}s^{-1}$]) [6] as,

$$N_{DIRC}[\text{kHz}] = 35 \cdot I_{LER} + 8.5 \cdot I_{HER} + 25 \cdot \mathcal{L}. \quad (3)$$

The occupancies extrapolated to high luminosities, assuming detector geometry and IR layout identical to that in BABAR, are given in Table II. Figure 4 shows the DIRC occupancies extrapolated for different luminosities indicating the individual contributions due to beam currents and luminosity. The DIRC occupancies in BABAR are acceptable up to $\mathcal{L} < 6\times10^{34}$ cm^{-2}s^{-1}. However, the water tank provides a huge Cherenkov detector. Thus, at luminosities $\mathcal{L} > 1\times10^{35}$ cm^{-2}s^{-1} the water tank has to be replaced with a compact readout system based on focusing and timing. Using pixelated photodetectors with a time resolution of < 200 ps should yield a factor of three improved Cherenkov-angle resolutions (2.7 mr) than achieved presently in the DIRC [3].

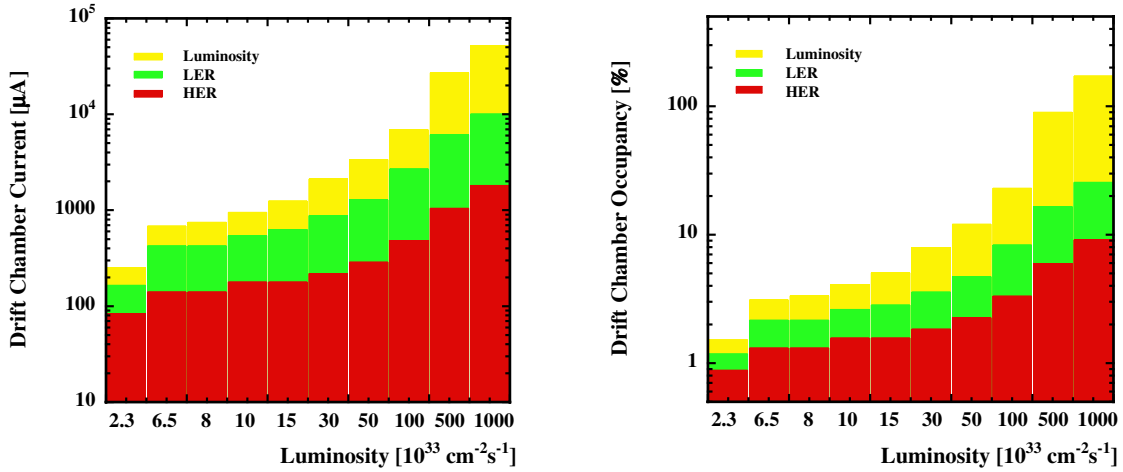

Figure 3: Projected drift chamber currents (left) and occupancy (right) for different luminosities. Individual contributions due to HER currents, LER currents and $\mathcal{L}$ are shown in logarithmic scale. Occupancies above 100% simply indicate that multiple hits are recorded per wire ($N_{hits} > N_{wire}$).

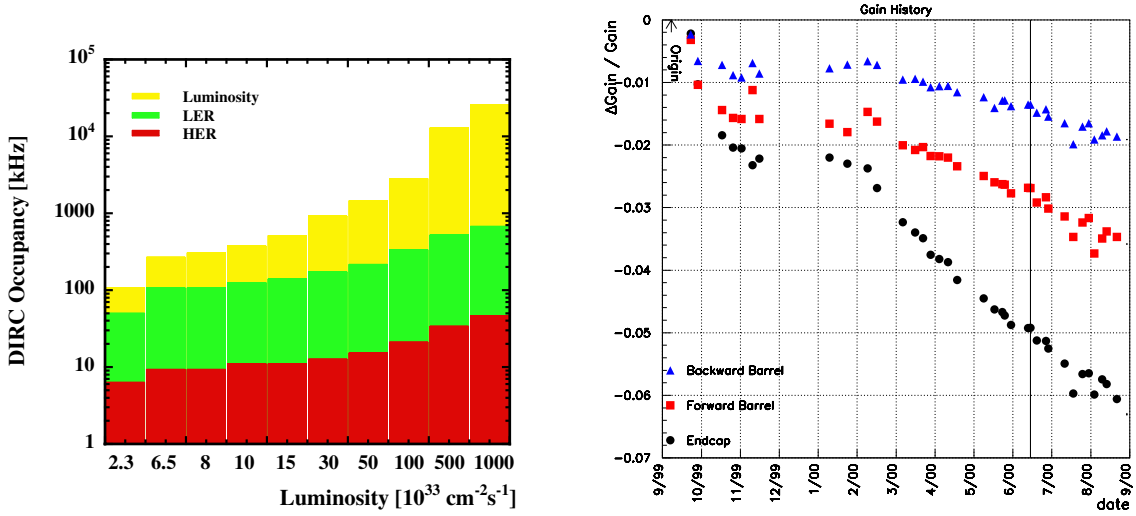

Figure 4: Projected DIRC occupancy for different luminosities showing individual contributions due to HER currents, LER currents and $\mathcal{L}$ in logarithmic scale (left). Observed light loss in different regions of the BABAR EMC (right).

6. Electromagnetic Calorimeter (EMC)

The performance of a thallium-doped CsI-crystal calorimeter is affected by radiation damage and occupancy. Radiation damage causes light losses, which first affect low-energy signals yielding increased inefficiencies. In the worst case the crystals are destroyed. Figure 5 shows the light-yield changes observed in the BABAR CsI(Tl)-crystal calorimeter. The forward endcap is most affected by radiation. At a dose of 160 Rad accumulated for an integrated luminosity of $\sim$ 23 fb^{-1} about 7.5% of the light is lost. In the forward and backward barrel about a 100 Rad have been accumulated yielding light losses of 4% and 2%, respectively. High occupancies may degrade the energy resolution of real photons and increase the combinatorial background in the π^0 mass spectrum. Figure 5 shows the single-crystal occupancy for crystals with a $\geq$ 1 MeV energy deposit and the number of crystals with energy E $\geq$ 10 MeV in the BABAR EMC as a function of beam currents. These measurements yield the following parameterizations in terms of beam currents ([A]) and $\mathcal{L}$ ([10^{33}cm^{-2}s^{-1}]) [6]:

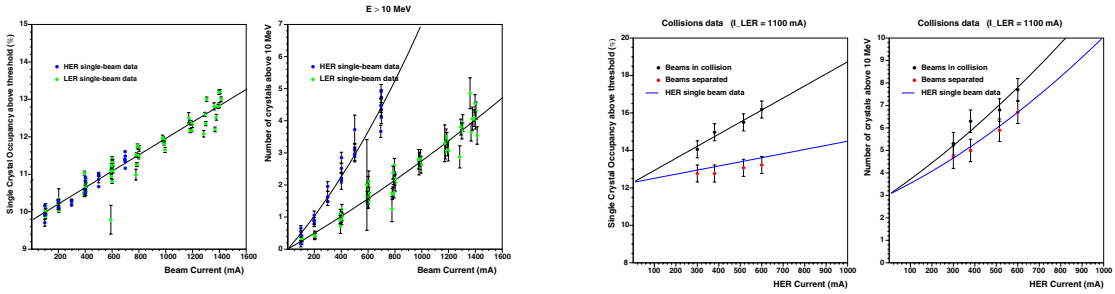

Figure 5: Single crystal occupancy for energy deposits of > 1 MeV and number of crystals with energies above 10 MeV observed in BABAR as a function of PEP II beam currents for single beams (left set) and two beams (right set).

$$\begin{aligned} O_{E>1\ \mathrm{MeV}}[\%] &= 9.8 + 2.2 \cdot I_{\mathrm{LER}} + 2.2 \cdot I_{\mathrm{HER}} + 1.4 \cdot \mathcal{L} \qquad (>1\ \mathrm{MeV}), \\ N_{E>10\ \mathrm{MeV}} &= 4.7 \cdot I_{\mathrm{HER}} + 0.23 \cdot I_{\mathrm{HER}}^2 + 2.4 \cdot I_{\mathrm{LER}} + 0.33 \cdot I_{\mathrm{LER}}^2 + 0.6 \cdot \mathcal{L} \quad (>10\ \mathrm{MeV}). \end{aligned} \tag{4}$$

Table II lists the extrapolated occupancies for different luminosities and Figure 6 shows the individual contributions due to beam currents and luminosity. The rapid rise of the luminosity term underscores the importance of properly handling the radiative Bhabha debris. For $\mathcal{L} < 1.5 \times 10^{34}$ cm^{-2}s^{-1} the integrated radiation dose in the BABAR CsI(Tl) calorimeter is unproblematic, if the observed light losses scale as expected. The impact of the large number of low-energy photons on the EMC energy resolution needs to be studied, as σ_E/E depends on the clustering algorithm, on digital filtering and a low-energy cut-off. Background rates can be reduced by improvements of the vacuum near the IR combined with effective collimation against e^+ from distant Coulomb scattering. For luminosities $\mathcal{L} > 1 \times 10^{35}$ cm^{-2}s^{-1} light losses due to radiation damage and occupancy levels in CsI(Tl) crystals are not acceptable. *R&D* is needed to find another inorganic scintillator that works in this environment. Candidates include pure CsI crystals read out with APS's, LSO or GSO read out with photodiodes or APD's. For example, LSO has interesting properties: a light yield of 27000 photons/MeV (compared to 56000 photons/MeV in CsI(Tl)), a radiation length $X_0 = 1.14$ cm, a Molière radius of 2.3 cm, and radiation hardness of 100 MRad [3]. Though LSO is a factor > 2 more expensive than CsI(Tl), LSO crystals may be cheaper than CsI(Tl) crystals, since the volume for the same X_0 and same angular segmentation is a factor of ~ 3.5 smaller.

7. Instrumented Flux Return (IFR)

The main issue for the IFR is the high occupancy in outer layers due to beam-related backgrounds. In BABAR, for $\mathcal{L} = 3 \times 10^{33}$ cm^{-2}s^{-1} the outer RPC layer has an occupancy of several %. At PEP II design currents this will already become unacceptable due to an enhanced μ/π misidentification. The solution is to build a 5 cm thick Fe shield behind the outermost layer of RPC chambers. This yields acceptable background rates for luminosities up to $\mathcal{L} = 3 - 5 \times 10^{34}$ cm^{-2}s^{-1}. Above $\mathcal{L} = 1 \times 10^{35}$ cm^{-2}s^{-1} occupancy levels become an issue despite the shielding. Scintillating fibers provide an alternative readout that may be considered here.

8. First-Level Trigger Rates (L1)

The first-level (L1) trigger rates in BABAR scale linearly with beam currents and luminosity as shown in Figure 7. The data can be parameterized by [6]

$$\mathrm{L1[Hz]} = 130\ (\mathrm{cosmics}) + 130 \cdot I_{\mathrm{LER}} + 360 \cdot I_{\mathrm{HER}} + 70 \cdot \mathcal{L}, \tag{5}$$

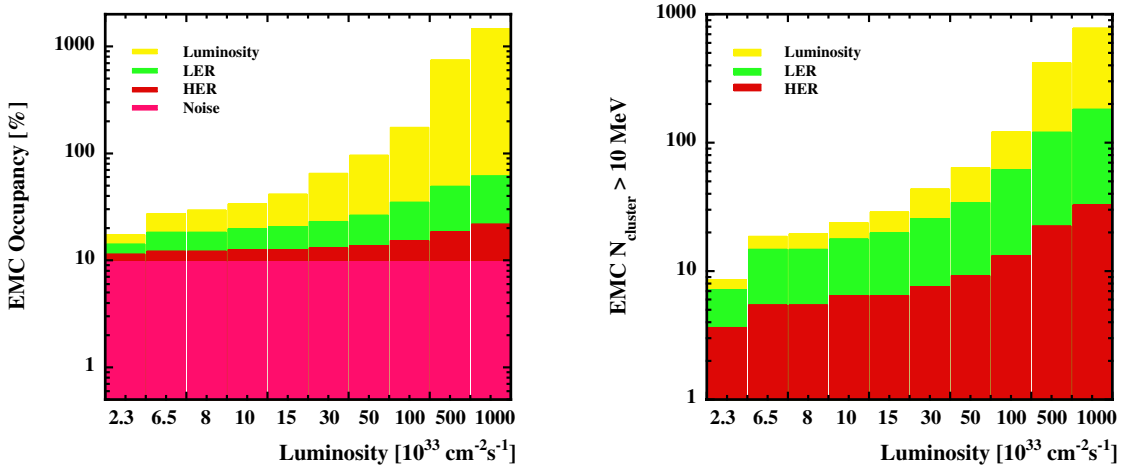

Figure 6: Single crystal occupancy for > 1 MeV energy deposits (left) and number of crystals with energies > 10 MeV (right) projected for different luminosities. Individual contributions due to noise, HER current, LER current and $\mathcal{L}$ are shown in logarithmic scale. Occupancies above 100% indicate multiple > 1 MeV showers overlapping in crystals ($N_{shower} > N_{crystal}$).

where beam currents and luminosity are given in units [A] and [10^{33} cm^{-2}s^{-1}], respectively. For high luminosities the last term dominates. The rates expected at high luminosities are listed in Table II. The different contributions to L1 are plotted in Figure 7. BABAR is laid out to accept an L1-trigger rate of 2.0-2.5 kHZ, depending on the event size. To operate BABAR at $\mathcal{L} > 1.5 \times 10^{34}$ cm^{-2}s^{-1} the L1 trigger needs to be upgraded. For luminosities $\mathcal{L} > 1 \times 10^{35}$ cm^{-2}s^{-1} a new trigger design is needed in order to accept the entire physics rate from $b\bar{b}$ and $c\bar{c}$ processes. This is important for analyses that require the full reconstruction of one B meson. However, we could apply a rather stringent prescaling of Bhabhas and radiative Bhabhas and reduce beam-gas events by maintaining a low pressure at and near the IR. At $\mathcal{L} = 1 \times 10^{36}$ cm^{-2}s^{-1} an L1-tigger rate of 75 kHz is expected. It should, however, be no problem of building a trigger system that can cope with such rates. For example the ATLAS trigger system is expected to accept an L1-trigger rate of 100 kHz. This is needed to minimize dead times for a 40 Mhz beam crossing rate.

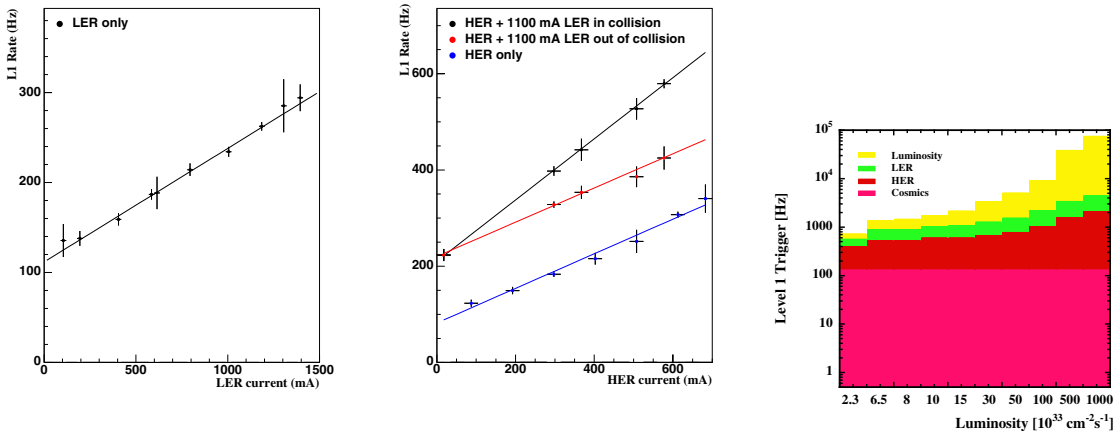

Figure 7: L1 trigger rate in BABAR versus LER (left) and HER beam currents (center); L1 trigger rates expected for different luminosities (right), showing individual contributions due to cosmic rays, beam currents and $\mathcal{L}$ in logarithmic scale.

9. Detector Considerations

Based on our present knowledge we have considered two detector scenarios: an upgraded BABAR detector and a new compact detector. In the first scenario we would keep the BABAR magnet, the flux return and the DIRC. The flux return would be instrumented with scintillating fibers and the DIRC with a compact readout system using focusing and timing to collect the Cherenkov photons in pixelated photon detectors [3]. The SVT, central tracker and electromagnetic calorimeter have to be rebuilt using one of the options discussed above. Furthermore, new trigger and data acquisition systems are necessary. Because of beam-focusing elements the angular detector acceptance in the super B factory is also limited to 300 mr as in PEP II. In order to improve the vertex resolution by a factor of two with respect to that in BABAR to achieve an improved separation of the two B decay vertices for the same boost ($\beta\gamma = 0.56$) as in PEP II, the beam pipe radius needs to be reduced to 1 cm. For a gold-plated Be beam pipe (1 cm radius, 20 cm length) the expected heat load is 0.5 MW from image current heating and 1 MW from incoherent higher-order modes (HMO) [10]. Using a double-wall beam pipe with 0.5 mm cooling channels and pumping water at a rate of 1.5 L/min sufficient cooling is achieved.

A possible choice of a compact detector which also utilizes the asymmetric beam energies is sketched in Figure 8. The tracking systems resides within a 50 cm radius. The SVT consists of a 2-layer Si-pixel plus a 3-layer Si-strip configuration and is followed by a 4-layer Si-strip central tracker. The SVT layers lie within 10 cm starting at a radius of 1.3 cm. All Si layers are bent inwards in the forward and backward directions to reduce the path length in the silicon. The DIRC starts at 50 cm and consists of a barrel and a forward endcap, which are respectively read out in the back and the front using a compact readout system. The EMC starts at ~ 60 cm. To maintain the same position resolution as in BABAR a scintillator with a reduced Molière radius is chosen, such as LSO which also has a shorter X_0 than CsI. The crystals may be segmented into two pieces to obtain longitudinal shower information which helps to separate hadron split-offs from photon showers. The crystals are read out with photodiodes or with APD's. To compensate for the short track length a magnetic field of 3 T is considered. The IFR starts at about 100 cm and stretches to 190 cm. It consists of eight 2.5 cm thick Fe layers interspersed with layers of scintillating fibers followed by seven 10 cm thick Fe layers interspersed with layers of scintillating fibers. In the beam direction the detector is 4.1 M long.

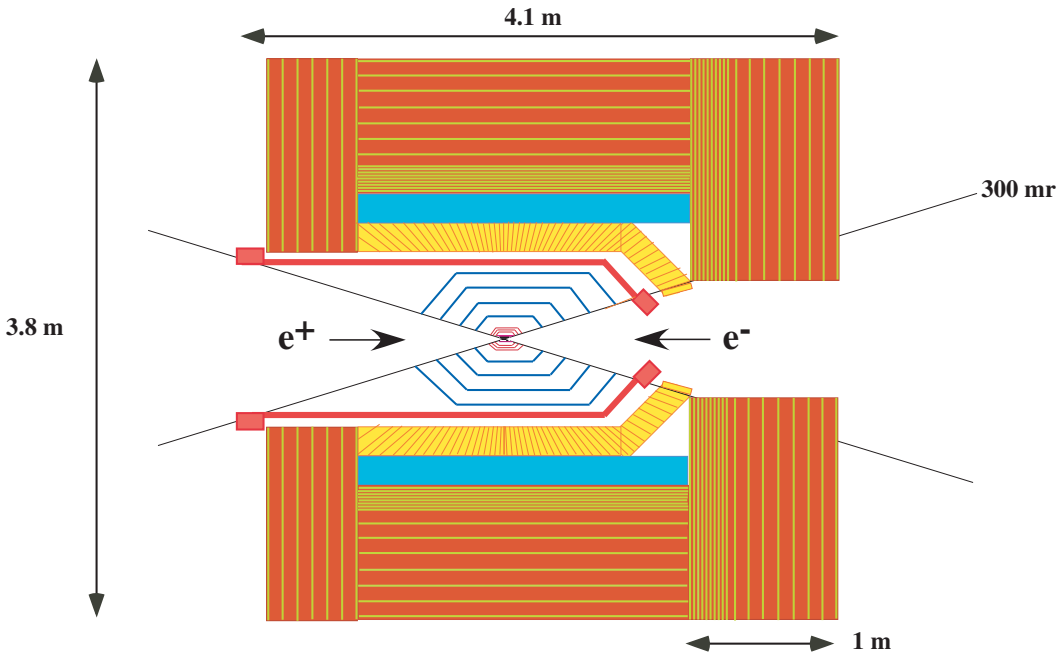

Figure 8: Side view of a compact multipurpose detector for a super B factory.

Table II Extrapolations of dose rates, currents and occupancies in detectors for different luminosities.

Machine	$\mathcal{L}_{peak}$ [$cm^{-2}s^{-1}$]	6.5×10^{33}	1.5×10^{34}	$5.\times10^{34}$	1×10^{35}	1×10^{36}
properties	$\int \mathcal{L}dt$ [fb^{-1}/y]	65	150	500	1000	10000
	I_{LER}/I_{HER} [A]	2.8/1.1	3.7/1.1	4.6/1.5	9/2.5	18/5.5
SVT	Dose D_{SVT} [kRad/y] for FE-MID/BW-MID	480/280	690/340	1300/470	2450/670	7490/1630
DCH	I_{DCH} [μA]	680	1250	3370	6880	51960
	$N_{DCH} = N_{hits}/N_{wires}$ [%]	3.1	5	12	23	173
	Q_{wire} [mC/cm]	~ 15	36	100	200	2000
DIRC	N_{DIRC} [kHz]	270	516	1470	2840	25700
EMC	$N_{EMC} = N_{shower}(> 1\ MeV)/N_{crystal}$ [%]	28	42	93	175	1460
	$N_{cluster}$	21	32	56	122	783
Trigger	$L1$ [Hz]	1350	2130	4800	9200	74500

10. Conclusion

A multipurpose detector can be built with existing or new technologies which exploits the unique physics opportunities at a super B factory operating at a luminosity of $\mathcal{L} = 1\times10^{36}$ $cm^{-2}s^{-1}$. For example, by performing precision measurements of rare decays [4] the super B factory is complementary to searches for New Physics in high-energy colliders. The detector requirements include good momentum resolution, high efficiency for low-momentum tracks, good photon-energy resolution, good position resolution of secondary vertices, a high K/π separation and a high μ efficiency with a low misidentification probability. To find optimal detector choices and construct a detector in a reasonable time scale $R\&D$ needs to be conducted in several areas soon.

Acknowledgments

This work has been supported by NFR. I would also like to thank W. Kozanecki for useful discussions.

References

[1] B. Aubert and *et al.* (BABAR collaboration), Phys. Rev. Lett. **87**, 091801 (2001).
[2] K. Abe and *et al.* (BELLE collaboration), Phys. Rev. Lett. **87**, 091802 (2001).
[3] P. Burchat and *et al.*, Physics at a 10^{36} Asymmetric B Factory, Proceedings of Snowmass Wokshop.
[4] G. Eigen, talk in P3-2 session, preprint P3-36, Proceedings of Snowmass Wokshop.
[5] J. Seeman, Proceedings of PAC2001.
[6] C. Harst and *et al.*, BaBar Note 522, 30 pp (2000).
[7] J. Seeman, SLAC-PUB-8787, March 2001; W. Kozanecki, internal note (2001).
[8] L. Andricek and *et al.*, Nucl. Instr. Meth. **A409**, 184 (1998).
[9] G. Lutz, Semiconductor Radiation Detectors, Springer Verlag (1999).
[10] H. Yamamoto, talk in E2 session, Proceedings of Snowmass Wokshop.
[11] B. Aubert and *et al.* (BABAR collaboration), hep-ex/0105044.